

Optical absorption and luminescence spectroscopy of U^{3+} in K_2LaX_5 ($X=Cl,Br,I$)

H. P. Andres, K. Krämer, and H.-U. Güdel

Institut für Anorganische, Analytische and Physikalische Chemie, Freiestraße 3, CH-3000 Bern 9, Switzerland

(Received 30 January 1996)

The title compounds were synthesized and high-resolution absorption and luminescence spectra measured in the near-infrared, VIS, and near UV regions. The visible absorption spectra are dominated by very intense $5f \rightarrow 6d$ bands overlapping with $f-f$ transitions. The onset of the first $f-d$ absorption is shifted from $46\,000\text{ cm}^{-1}$ in $K_2LaCl_5:Nd^{3+}$ to $15\,000\text{ cm}^{-1}$ in $K_2LaCl_5:U^{3+}$. Crystal-field splittings in corresponding $^{2S+1}L_J$ multiplets are greater by typically a factor of 2 in the U^{3+} doped crystal, thus reflecting the larger extension and stronger interaction of the $5f$ electrons with the ligands. $f-f$ transitions are typically two orders of magnitude more intense in $K_2LaCl_5:U^{3+}$ than in $K_2LaCl_5:Nd^{3+}$. Along the halide series $K_2LaX_5:U^{3+}$ ($X=Cl,Br,I$) the differences in the position of corresponding $f-d$ and $f-f$ transitions, crystal-field splittings, vibronic intensities, and excited-state lifetimes can be explained with the increasing covalency, the decreasing phonon energies, the increasing electron-phonon coupling, and the increasing U-X distances. The $f-d$ excited states provide a nonradiative bypass of some $f-f$ excited states in the case of all these halide lattices. The excited-state dynamics are determined by a delicate interplay of radiative and nonradiative relaxation processes, they are strongly dependent on the nature of X . Multiphonon relaxation processes are least competitive in the iodide due to the very low value of 106 cm^{-1} for the highest-energy phonons. A cross-relaxation mechanism determines the dynamics of the iodide at room temperature. [S0163-1829(96)01530-5]

I. INTRODUCTION

The optical spectroscopy of trivalent actinide ions has received very little attention in comparison to the corresponding lanthanides. The physical instability of most actinide elements is an obvious reason, but by no means the only one. The actinides have a rich redox chemistry, quite in contrast to the lanthanides, in which the trivalent oxidation state is predominant. Thus, uranium forms chemically stable species in the oxidation states $2+$, $3+$, $4+$, $5+$, and $6+$. Attempts to produce U^{3+} -doped crystals by high-temperature synthesis thus often yield products containing uranium in more than one oxidation state.

The early studies on U^{3+} -doped crystals around 1960 were stimulated by their potential use as IR-laser materials. Extensive studies were carried out with U^{3+} doped in CaF_2 , SrF_2 , and BaF_2 .¹⁻³ But the coexistence of other valence states and multiple sites led to some confusion and discrepancies in interpretation of the observed data. In the early 1970's a single study on the compound $U(HCOO)_3$ was published, which contained a parametric analysis of the energy splitting in the region of $f-f$ transitions.⁴ The effective Hamiltonian used in Ref. 4 consisted of an electrostatic, a spin-orbit, and a configuration-interaction part, and parameters describing these interactions were obtained by a least-squares fit. The analysis was only based on absorption spectra. At the end of the 1970's the luminescent behavior of a single level in U^{3+} -doped $LaBr_3$ was studied in detail.⁵ The presence of multiple sites was nicely demonstrated. In 1979 and 1980 two papers, completing and summarizing the knowledge about U^{3+} -doped $LaCl_3$ were published.^{6,7} They included extensive luminescence and absorption spectra, as well as fits to the $f-f$ energy levels with an effective Hamiltonian. From these fits electrostatic, spin-orbit, configurational, and crystal-field interaction parameters including

magnetically correlated correction terms were derived. These parameters were put in relation to values of the other actinides in the same host.⁸ A most recent study also considered the pressure dependence in the parameters.⁹ Another host lattice doped with trivalent uranium was Cs_2NaYCl_6 , which was investigated in 1988.¹⁰ In this publication and a later one¹¹ the shape of the $f-d$ absorption was qualitatively assigned in the limit of strong interaction between f and d electrons. An extensive study, including detailed analysis at low temperature in absorption showed the difficulty to assign the observed transitions due to strong vibronic sidebands.¹² After these more fundamental studies, attention was again directed to laser material applications. The high emission cross section of the transition $^4I_{11/2} \rightarrow ^4I_{9/2}$ and the strong splitting of the ground state make U^{3+} -doped $LiYF_4$ a very promising four-level IR-laser material, operating around $2.8\text{ }\mu\text{m}$.¹³⁻¹⁵ This emission can be pumped either in the strong $f-d$ or $f-f$ absorption bands. The coexistent U^{4+} quenches the U^{3+} emission by reabsorption, but by irradiation of the crystals with γ rays the U^{4+} valence state is eliminated. Very recently a parametric energy analysis, analogous to the one of $LaCl_3:U^{3+}$ was published.¹⁶

The present study of U^{3+} -doped K_2LaX_5 ($X=Cl,Br,I$) was motivated by several reasons. First, we were impressed by the small number of optical spectroscopic studies of U^{3+} in the literature, all on randomly chosen host lattices. The title compounds are isostructural, and by the chemical variation $X=Cl \rightarrow Br \rightarrow I$ we can study the resulting trend in the optical spectroscopic properties. Such a comparative investigation has not been done before, to our knowledge. The inclusion of the iodide is particularly interesting, because the optical spectroscopic properties of U^{3+} in this environment are completely unexplored and within the halide series it represents by far the most covalent bonding situation. The undiluted pure compounds K_2UX_5 ($X=Cl,Br,I$) have re-

TABLE I. Experimental parameters used in the Bridgman crystal growth.

Compound	Starting temperature (°C)	Cooling rate (°C/h)	Till temperature (°C)	Cooling rate (°C/h)	End temperature (°C)
$\text{K}_2\text{LaCl}_5:\text{U}^{3+}$	660	2	450	10	20
$\text{K}_2\text{LaCl}_5:\text{Nd}^{3+}$	640	2	450	10	20
$\text{K}_2\text{LaBr}_5:\text{U}^{3+}$	800	2	450	10	20
$\text{K}_2\text{LaI}_5:\text{U}^{3+}$	550	2	450	10	20

cently been synthesized and studied in detail.^{17–19} They are isostructural to K_2LaX_5 with only one metal site per unit cell, and the synthesis of mixed crystals with a well-defined U^{3+} oxidation state is possible. Many of the earlier studies had been hampered by the presence of multiple sites or the coexistence of uranium in other oxidation states.^{1,2,5,6,15} No such evidence was found in our experiments on the title compounds. Besides the variation of the host lattice we found another comparison most interesting, namely the substitution of the $(5f)^3$ ion U^{3+} by the $(4f)^3$ ion Nd^{3+} in the same host lattice. This relates the poorly investigated area of $5f$ spectroscopy to the well-established area of $4f$ spectroscopy. Besides the energetic aspects we were interested in the excited-state dynamics in U^{3+} -doped K_2LaX_5 ($X=\text{Cl,Br,I}$) and their dependence on the variable X .

II. EXPERIMENTAL

A. Crystal preparation

Starting materials for the synthesis of $\text{K}_2\text{LaX}_5:\text{U}^{3+}$ ($X=\text{Cl,Br,I}$) were KX , LaX_3 , and K_2UX_5 . The potassium halides were purchased [E. Merck, suprapure]. To remove water and oxygen they were purified by sublimation in a tantalum ampoule. LaCl_3 and LaBr_3 were prepared from La_2O_3 , following the ammonium halide route.²⁰ LaI_3 was synthesized from the elements.²¹ The preparation of the pure K_2UX_5 was earlier described in detail.¹⁸ Mixed crystals were grown by mixing appropriate amounts of the starting materials in a tantalum ampoule and using the Bridgman technique with the parameters shown in Table I. The preparation of $\text{K}_2\text{LaCl}_5:\text{Nd}^{3+}$ is slightly different. The starting materials KCl , LaCl_3 , and K_2NdCl_5 were mixed in a silica ampoule, and the Bridgman growth parameters are included in Table I. The nominal dopant concentration was 1 mol % for $\text{K}_2\text{LaBr}_5:\text{U}^{3+}$, $\text{K}_2\text{LaI}_5:\text{U}^{3+}$, and $\text{K}_2\text{LaCl}_5:\text{Nd}^{3+}$ and 0.8 mol % for $\text{K}_2\text{LaCl}_5:\text{U}^{3+}$, respectively. The effective U^{3+} concentration in the iodide lattice is expected to be lower, because indications of K_2UI_5 decomposition were observed during the crystal growth. The products were characterized by x-ray powder diffraction.

B. Absorption spectra

Crystals were selected, cut, and polished to a defined thickness in a nitrogen dry box. For the absorption measurements, they were mounted into a gas tight copper cell with silica windows and cooled to 14 K with a closed-cycle helium refrigerator. The orientation of the crystals was random. The low site symmetry of the luminescent centers makes information obtained by polarized measurements not inter-

pretable. The absorption spectrum of $\text{K}_2\text{LaCl}_5:\text{U}^{3+}$ was measured on a Cary 17 from 4000–26 000 cm^{-1} . The absorption spectra of $\text{K}_2\text{LaCl}_5:\text{Nd}^{3+}$, $\text{K}_2\text{LaBr}_5:\text{U}^{3+}$, and $\text{K}_2\text{LaI}_5:\text{U}^{3+}$ were measured on a Cary 5E. For the uranium (III)-doped crystals additional spectra in the range of 10 000 to 15 000 cm^{-1} were recorded with a high-resolution double beam spectrometer based on a Spex 1401 double monochromator and a Hamamatsu R406 photomultiplier tube.

C. Luminescence spectra

For the luminescence measurements polycrystalline samples were sealed under a helium atmosphere into thin walled glass tubes. These samples were placed in a silica flow tube and cooled in a helium gas stream, produced by the boiloff of liquid helium. After pulsed second harmonic YAG: Nd^{3+} (Spectra-Physics Quanta-Ray DCR-3) laser excitation at 532 nm, luminescence was dispersed in a Spex 1702 monochromator and recorded by a Stanford Research photon counting system SR400, using a RCA C31034 photomultiplier tube for the 650–900 nm region. IR luminescence was recorded after excitation at 568.2 nm with a Kr^+ laser (Coherent Innova 300) by a lock-in amplifier (SRS M 501), using the chopped signal of a cooled Ge detector ADC403L (900–1600 nm) or a cooled PbS diode Hamamatsu P3337 (1600–2600 nm). In addition, the overlap region from 650 to 1100 nm was measured by Kr^+ -laser excitation at 568.2 nm, the Standard Research photon counting system SR400, and a Hamamatsu R406 photomultiplier tube. An AT-compatible computer was used for monochromator control and data acquisition.

D. Lifetime measurements

For the luminescence lifetime measurements excitation was achieved with the second harmonic at 532 nm of the pulsed YAG: Nd^{3+} laser. For the detection a fast Ge detector (ADC403HS, 1 μs response) was used together with a digital oscilloscope (Tektronix TDS 540A), which was also used for the data acquisition.

E. Data treatment

The data were analyzed using Igor (Wave Metrics). The luminescence spectra were corrected for the wavelength dependence of the instrumental response. A tungsten halogen lamp was used to illuminate the spectrometer slit and the photon count rate recorded with constant nm spectral bandwidth over the whole wavelength range. These photon count rates were then divided by the photon flux per nm s (J_λ) for a black body at 3300 K calculated from the expression

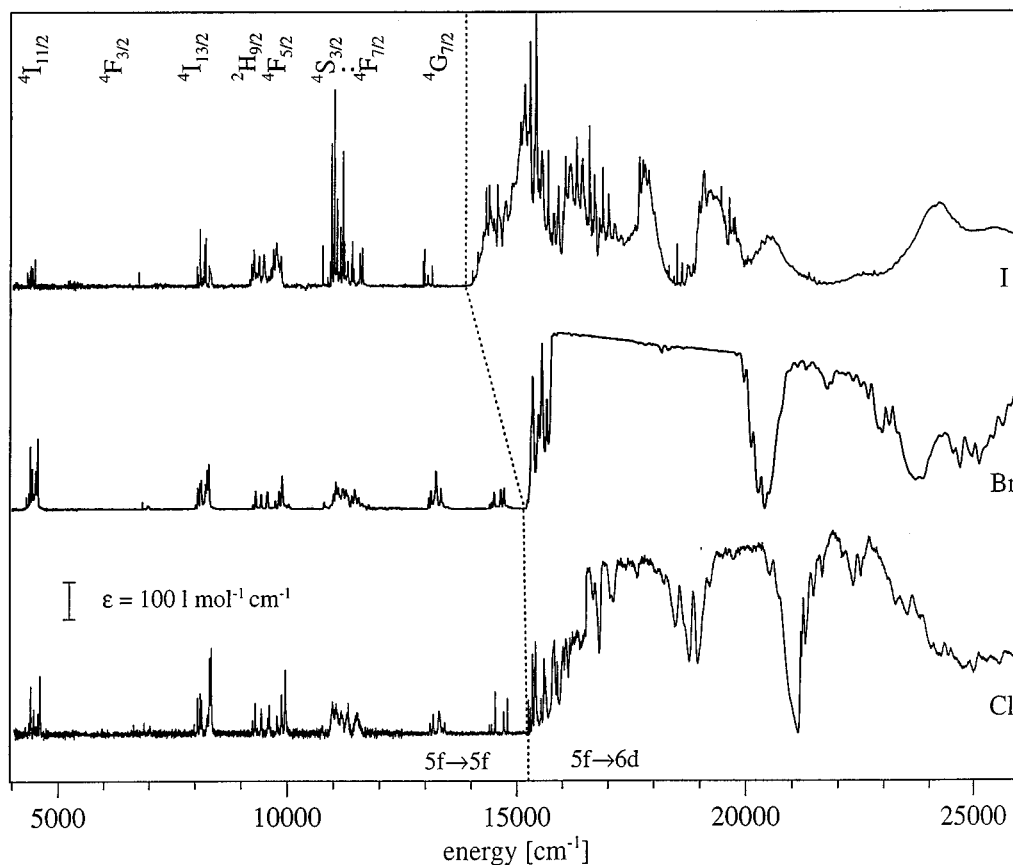


FIG. 1. Measured overall NIR/VIS absorption spectra at 14 K of $K_2LaX_5:U^{3+}$ ($X=Cl, Br, I$). The onset of the $5f \rightarrow 6d$ absorptions is marked by a broken line. The $f-f$ transitions are labeled by the $^{2S+1}L_J$ labels of the excited states.

$J_\lambda = 2\pi c \lambda^{-4} [\exp(hc/\lambda kT) - 1]^{-1}$ to yield an array of relative instrumental response factors at unit wavelength intervals.²² By dividing the experimental spectrum by this array we obtain a spectrum in $nm^{-1} s^{-1}$ vs nm . This spectrum is then converted in photon flux per $cm^{-1} s$ (J_E) vs cm^{-1} by using the appropriate y -axis transformation from Ejder.²² By normalizing the band areas in the overlapping regions of the spectra obtained for the same sample with different detectors an overview spectrum is obtained.

III. RESULTS

A. High-resolution spectroscopy

Figure 1 shows the unpolarized low-resolution absorption spectra of $K_2LaX_5:U^{3+}$ ($X=Cl, Br, I$) at 14 K. Two absorption regions, which are separated by a broken line in Fig. 1, can be clearly distinguished. On the red side of this demarcation the spectrum consists of sharp line multiplets down to 4000 cm^{-1} . These absorptions can be readily assigned to transitions within the $(5f^3)$ electron configuration, and the multiplets can be labeled from comparison with the literature. The multiplet energies tend towards smaller values in the series $Cl \rightarrow Br \rightarrow I$, but the total shift of the baricenters is 207 cm^{-1} at most. On the blue side of the broken line in Fig. 1 the sharp $f-f$ transitions are superimposed by absorptions which are much broader and more intense by about two orders of magnitude. The most intense absorptions in the Cl and Br crystal are limited by straylight. The onset of these

$5f \rightarrow 6d$ excitations show a redshift of approximately 1000 cm^{-1} between Cl and I. These absorptions extend from the VIS up into the near UV and the structure is similar in the three lattices.

After excitation at 532 nm in the broad absorption band luminescence from several $f-f$ states is observed. For the three lattices at 14 K this is shown in Fig. 2. The sharp multiplets are readily assigned as shown in the figure. The $^4G_{7/2} \rightarrow ^4I_{9/2}$ luminescence is magnified under high resolution in Fig. 3. We note a slight redshift of the multiplet baricenter, a decrease of the overall crystal-field splitting, and an increase of the vibronic intensity in the series $Cl \rightarrow Br \rightarrow I$. We also note that the intensity distribution among the crystal-field components does not vary significantly along the series. These trends are found in all the multiplets of the luminescence spectrum. The origins of all the corresponding multiplets coincide in absorption and emission. We conclude that the electronic origins carry most of the intensity. On this basis we derive the energy levels listed in Table II from a full analysis of the absorption and luminescence spectra. The energy differences between the crystal-field components of the multiplets are also listed. We observe a decrease of 11 to 49 % between Cl and I.

Figure 4 compares the absorption spectra of $K_2LaCl_5:U^{3+}$ and $K_2LaCl_5:Nd^{3+}$ at 14 K. Transitions to the 4I , 4G , and 4F multiplets are indicated in the spectra. In the Nd^{3+} spectrum these multiplets are well separated from each other, whereas in the U^{3+} spectrum a considerable

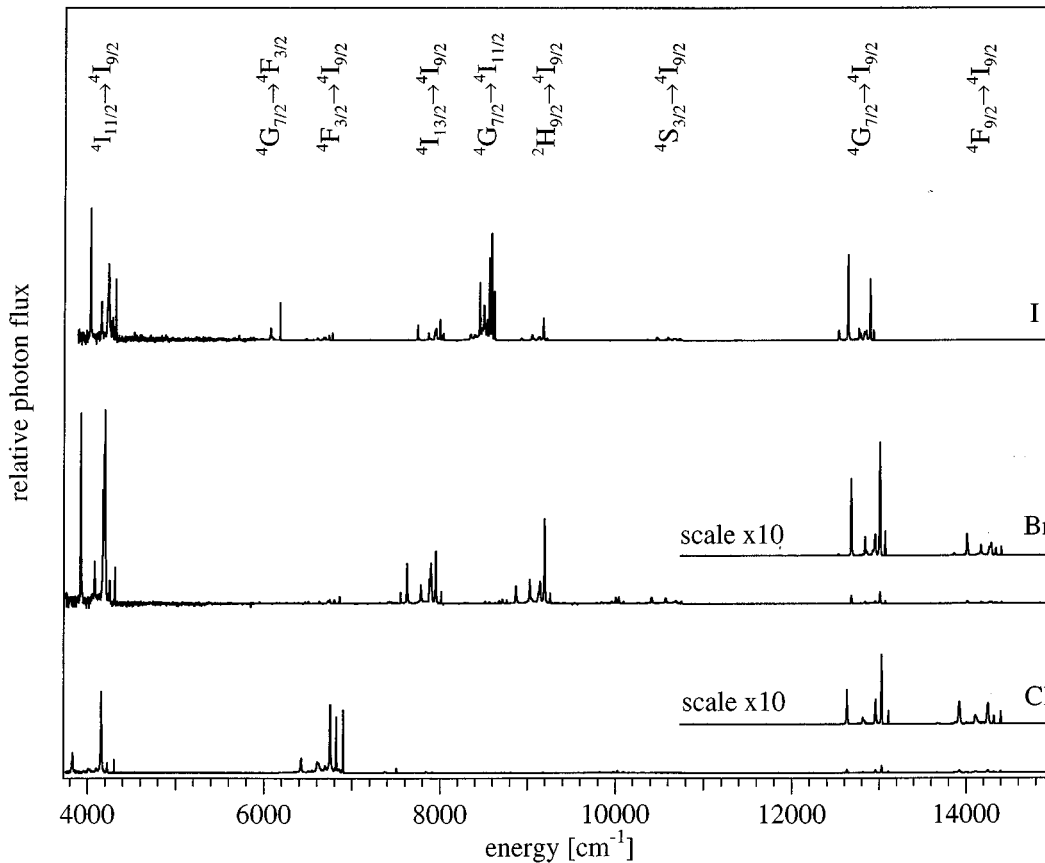


FIG. 2. Overall IR/VIS luminescence spectra of $\text{K}_2\text{LaX}_5:\text{U}^{3+}$ ($X=\text{Cl}, \text{Br}, \text{I}$) at 14 K after excitation in a $f-d$ absorption band. For $X=\text{Br}, \text{Cl}$ an enlarged view of the region between 11 000 and 15 000 cm^{-1} is shown. Assignments of the multiplets are given at the top. The three intensity scales can vary by up to 50%.

overlap is observed. The most obvious difference between the two spectra, however, is the onset of the lowest $f-d$ absorption band, which lies around 15 000 and 46 000 cm^{-1} in the U^{3+} - and Nd^{3+} -doped crystals, respectively. The inset in Fig. 4 shows in detail one particular $f-f$ transition for both

compounds, namely ${}^4\text{I}_{9/2} \rightarrow {}^4\text{F}_{9/2}$. Note the change in scale, because the U^{3+} transitions are one to two orders of magnitude more intense than the corresponding Nd^{3+} transitions. The total crystal-field splitting of the ${}^4\text{F}_{9/2}$ is more than twice as large in the U^{3+} compound. Energies and energy splittings of the $f-f$ levels derived from the absorption spectrum of $\text{K}_2\text{LaCl}_5:\text{Nd}^{3+}$ are included for comparison in Table II.

Luminescence spectra of all the U^{3+} compounds were recorded at three different temperatures, namely at 14, 80, and 280 K. Table III lists the relative intensities of the various multiplet luminescences. There is a general intensity decrease with increasing temperature, but the relative intensities remain more or less the same. The iodide represents a notable and significant exception, which is shown in Fig. 5. At 280 K we observe a drastic reduction of all intense low-temperature multiplets and a concomitant enormous rise of the ${}^4\text{S}_{3/2} \rightarrow {}^4\text{I}_{9/2}$ luminescence around 11 000 cm^{-1} , see also Table III.

B. Time-resolved measurements

The decay curve of the ${}^4\text{F}_{3/2}$ luminescence is single exponential in all three lattices and the lifetimes in Table IV were derived for 14 and 280 K, respectively. Besides this transition, none of the other luminescences showed a single exponential decay in the chloride and bromide lattice. In the iodide, on the other hand, all the luminescences decay expo-

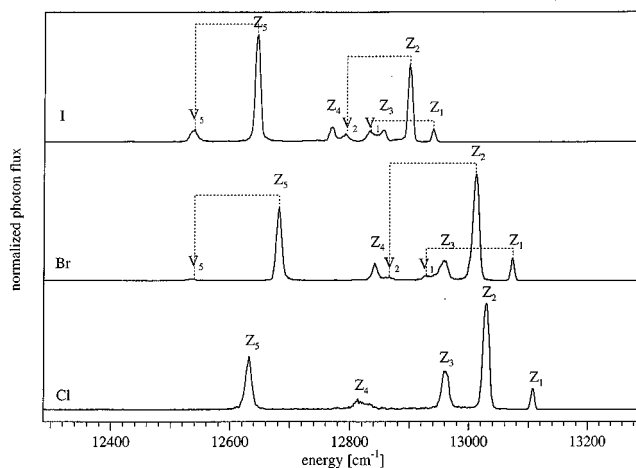


FIG. 3. A detailed view for the three host lattices of the ${}^4\text{G}_{7/2} \rightarrow {}^4\text{I}_{9/2}$ luminescence transition at 14 K, after excitation at 532 nm into the $f-d$ band. Assignments of the origins to the labels Z_i is made according to Table II and vibronic sidebands are labeled V_i accordingly.

TABLE II. f - f energy levels and energy splittings ΔE (cm^{-1}) in $\text{K}_2\text{LaX}_5:\text{U}^{3+}$ ($X=\text{Cl,Br,I}$) and $\text{K}_2\text{LaCl}_5:\text{Nd}^{3+}$ derived from absorption and luminescence spectra, with an experimental error of $1\text{--}2\text{ cm}^{-1}$. The symbols are chosen according to Ref. 6.

$2S+1L_J$	Symbol	$\text{K}_2\text{LaCl}_5:\text{U}^{3+}$		$\text{K}_2\text{LaBr}_5:\text{U}^{3+}$		$\text{K}_2\text{LaI}_5:\text{U}^{3+}$		$\text{K}_2\text{LaCl}_5:\text{Nd}^{3+}$	
		ΔE	ΔE	ΔE	ΔE	ΔE	ΔE		
$^4I_{9/2}$	Z_1	0		0		0			
	Z_2	78		61		39			
	Z_3	145		114		84			
	Z_4	294		231		170			
	Z_5	475		391		293			
$^4I_{11/2}$	Y_1	4298		4308		4317			
	Y_2	4368	70	4358	50	4349	32		
	Y_3	4410	112	4395	87	4374	57		
	Y_4	4475	177	4442	134	4399	82		
	Y_5	4568	270	4509	201	4437	120		
	Y_6	4614	316	4556	248	4484	167		
$^4F_{3/2}$	X_1	6897		6857		6770		10 862	
	X_2	7032	135	6978	121	6860	90		
$^4I_{13/2}$	W_1	7985		8016		8043		3854	
	W_2	8059	74	8064	48	8063	20	3903	49
	W_3	8115	130	8116	100	8106	63	3941	87
	W_4	8151	166	8142	126	8126	83	3959	105
	W_5	8279	294	8231	215	8168	125	4032	178
	W_6	8323	338	8266	250	8200	157	4058	204
	W_7	8356	371	8304	288	8234	191	4086	232
$^2H_{9/2}$	A_1	9254		9264		9228		12 476	
	A_2	9313	59	9319	55	9282	53	12 520	44
	A_3	9443	189	9439	175	9392	164	12 544	68
	A_4	9585	331	9561	297	9485	257	12 599	123
	A_5	9618	364	9582	318	9504	276	12 631	155
$^4F_{5/2}$	A_6	9782		9748		9653		12 347	
	A_7	9884	102	9825	77	9699	46	12 396	49
	A_8	9967	185	9891	143	9756	103	12 438	91
$^4S_{3/2}$	B_1	10 785		10 813		10 775		13 446	
	B_2	10 824	39	10 841	28	10 795	20	13 456	10
$^4G_{5/2}$	C_1	11 020		11 014		10 935		16 899	
	C_2	11 082	62	11 062	48	10 969	34	16 993	94
	C_3	11 122	102	11 110	97	11 026	91	17 031	132
$^4I_{15/2}$	D_1	11 188		11 144		11 087		5834	
	D_2	11 227	39	11 233	89	11 160	73	5893	59
	D_3	11 346	158	11 282	138	11 215	128	5940	106
	D_4	11 446	258	11 321	177	11 242	155	5963	129
	D_5	11 520	332	11 410	266	11 319	232	6126	292
	D_6	11 536	348	11 467	323	11 394	307	6159	325
	D_7	11 597	409	11 497	353	11 418	331	6164	330
	D_8	11 634	446	11 562	418	11 451	354	6188	354
$^4F_{7/2}$	E_1	11 701		11 634		11 551		13 301	
	E_2	11 758	57	11 682	48	11 585	34	13 346	45
	E_3	11 792	91	11 725	91	11 635	84	13 372	71
	E_4	11 872	171	11 775	141	11 658	107		
$^4G_{7/2}$	F_1	13 109		13 075		12 942		18 840	
	F_2	13 173	64	13 125	50	12 981	39	18 881	41
	F_3	13 428	319	13 340	265	13 051	109	18 920	80
	F_4					13 144	202	18 941	101
$^4F_{9/2}$	G_1	14 393		14 405				14 563	
	G_2	14 440	47	14 449	44			14 602	39
	G_3	14 524	131	14 502	97			14 633	70
	G_4	14 709	316	14 652	247			14 704	141
	G_5	14 793	400	14 720	326			14 750	187
$^2H_{11/2}$	H_1			15 234				15 814	

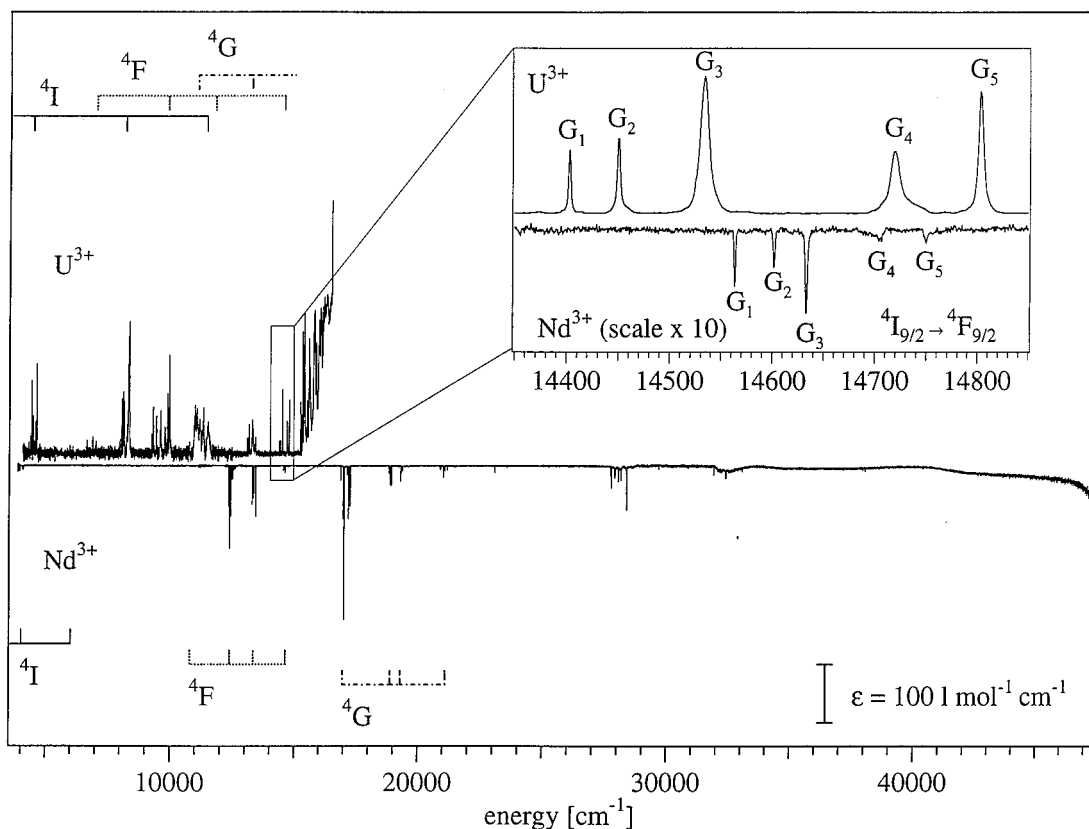


FIG. 4. Comparison of the overall absorption spectra at 14 K of $\text{K}_2\text{LaCl}_5:\text{U}^{3+}$ and Nd^{3+} , the Nd^{3+} spectrum is shown upside down. The 4I , 4F , and 4G multiplets are indicated for both compounds. The inset shows an enlarged view of the $^4I_{9/2} \rightarrow ^4F_{9/2}$ transition for both compounds, which is assigned according to Table II.

nentially at all temperatures. The lifetimes are collected in Table V. The transients of the $^2H_{9/2}$ luminescence in $\text{K}_2\text{LaCl}_5:\text{U}^{3+}$ are shown semilogarithmically in Fig. 6 for three temperatures. The inset of this figure gives a detailed view of the transient at 280 K on a nonlogarithmic scale. It shows an initial fast decay followed by a slow build-up and decay of the luminescence.

IV. DISCUSSION

A. General features

Trivalent uranium exhibits an extremely rich spectroscopy in the IR, VIS, and near UV spectral region in the title compounds. The undiluted compounds K_2UX_5 ($X=\text{Cl}, \text{Br}, \text{I}$) are very intensely colored, and even in the compounds reported here with a 1:100 dilution of U^{3+} the absorption spectrum is limited by straylight in the region of $f-d$ absorptions. The colors of K_2UX_5 ($X=\text{Cl}, \text{Br}, \text{I}$) are dark red, red violet, and blue, respectively.

Whereas in the spectroscopy of lanthanides there is a very clear distinction between “allowed” $f-d$ and “forbidden” $f-f$ transitions, this is somewhat blurred in the spectra reported here. This is mainly the result of the spin-orbit coupling and the odd-parity crystal field. The result is very clearly seen in Fig. 1. The $f-f$ absorptions are weaker than the $f-d$ absorptions by one to two orders of magnitude. In trivalent lanthanides this difference is typically three to four orders of magnitude. The rich fine structure observed in the

$f-d$ region of our spectra is thus the result of overlapping sharp $f-f$ and broad $f-d$ transitions.

Electron-repulsion and spin-orbit coupling are of the same order of magnitude in U^{3+} . Thus neither a SLJ nor a jjJ coupling scheme leads to an adequate labeling of the wave functions. In accordance with the literature and in analogy to the trivalent lanthanides we choose $^{2S+1}L_J$ labels for our multiplets. The actual wave functions are linear combinations of the $^{2S+1}L_J$ basis functions, and the $^{2S+1}L_J$ label used here represents the main component. This is a very practical choice, particularly for a comparison of the $f-f$ energy levels of $\text{Nd}^{3+}(4f^3)$ and $\text{U}^{3+}(5f^3)$.

As in the lanthanides, the optically active electrons in the $5f$ shell of U^{3+} are shielded by the spatially more expanded $6s$ and $6p$ electrons. Nevertheless, we expect stronger interactions of the $5f$ electrons with the surroundings due to their greater radial expansion compared to $4f$ systems. Thus the effect of chemical variation of the lattice on the energy levels are expected to be more pronounced. In the following sections the effects of two chemical variables on these properties are discussed.

B. Comparison of trivalent neodymium and uranium

A comparison of the optical spectroscopic properties of Nd^{3+} and U^{3+} in LaCl_3 has been reported in Ref. 7, but this was restricted to $f-f$ excitations. The most obvious difference in the VIS/UV absorption spectrum of Nd^{3+} - and U^{3+} -doped K_2LaCl_5 in Fig. 4 is the energy of the $f-d$ ab-

TABLE III. Relative intensities (in units photon flux J_E per cm^{-1} s) of the observed luminescence transitions in all three compounds at three temperatures. The most intense transition at 14 K was arbitrarily set to 100 for each compound.

Compound	Transition	Temperature (K)		
		14 K	80 K	280 K
$\text{K}_2\text{LaCl}_5:\text{U}^{3+}$	${}^4F_{9/2} \rightarrow {}^4I_{9/2}$	5	7	1
	${}^4G_{7/2} \rightarrow {}^4I_{9/2}$	7	5	1
	${}^2H_{9/2} \rightarrow {}^4I_{9/2}$	1	1	0
	${}^4I_{13/2} \rightarrow {}^4I_{9/2}$	1	1	0
	${}^4F_{3/2} \rightarrow {}^4I_{9/2}$	100	100	89
	${}^4I_{11/2} \rightarrow {}^4I_{9/2}$	35	47	31
$\text{K}_2\text{LaBr}_5:\text{U}^{3+}$	${}^4F_{9/2} \rightarrow {}^4I_{9/2}$	2	4	0
	${}^4G_{7/2} \rightarrow {}^4I_{9/2}$	4	9	2
	${}^4S_{3/2} \rightarrow {}^4I_{9/2}$	2	1	0
	${}^2H_{9/2} \rightarrow {}^4I_{9/2}$	38	32	16
	${}^4I_{13/2} \rightarrow {}^4I_{9/2}$	44	53	31
	${}^4F_{3/2} \rightarrow {}^4I_{9/2}$	4	1	1
$\text{K}_2\text{LaI}_5:\text{U}^{3+}$	${}^4F_{9/2} \rightarrow {}^4I_{9/2}$	0	0	2
	${}^4G_{7/2} \rightarrow {}^4I_{9/2}$	59	109	27
	${}^4G_{7/2} \rightarrow {}^4I_{11/2}$	100	139	6
	${}^4G_{7/2} \rightarrow {}^4F_{3/2}$	6	11	0
	${}^4S_{3/2} \rightarrow {}^4I_{9/2}$	0	1	364
	${}^2H_{9/2} \rightarrow {}^4I_{9/2}$	12	33	3
	${}^4I_{13/2} \rightarrow {}^4I_{9/2}$	20	33	4
	${}^4F_{3/2} \rightarrow {}^4I_{9/2}$	4	7	0
	${}^4I_{11/2} \rightarrow {}^4I_{9/2}$	86	154	23

sorptions. The onset to the lowest-energy f - d band is shifted from about $46\,000\text{ cm}^{-1}$ in Nd^{3+} to about $15\,000\text{ cm}^{-1}$ in the U^{3+} -doped crystal. This is primarily due to the fact that the energy difference between the $5f$ and $6d$ atomic orbitals is significantly smaller than the energy difference between $4f$ and $5d$. This effect is characteristic for the two metal ions involved and not their chemical environment and a similar difference is expected in the bromide or iodide lattice. Turning now to the f - f excitations, we first neglect the crystal-field splittings and discuss the multiplet energies. Taking the baricenters of the 4I_J , 4F_J , and 4G_J multiplets we see on the left-hand side of Fig. 4 that their energy differences are reduced by typically one third for U^{3+} compared to Nd^{3+} . This is a reflection of the smaller electron repulsion in U^{3+} , a very similar reduction was observed in U^{3+} - and Nd^{3+} -doped LaCl_3 .^{6,23} a value of the Slater radial integral F_2 of 319.4 and 176.5 cm^{-1} was estimated for U^{3+} and Nd^{3+} , respectively. The spin-orbit splitting of a given ${}^{2S+1}L$ term, on the other hand is larger by about one third for U^{3+} , thus reflecting the larger spin-orbit coupling parameters ($\xi_{nf}=1623\text{ cm}^{-1}$ versus 880 cm^{-1} for U^{3+} and Nd^{3+} ions in LaCl_3 , respectively^{6,23}). In combination these two effects lead to an overlap of the 4I_J , 4F_J , and 4G_J multiplets in U^{3+} , whereas in Nd^{3+} they are well separated, see Fig. 4.

The inset of Fig. 4 illustrates the effect of the crystal field on the ${}^4F_{9/2}$ term for U^{3+} and Nd^{3+} in K_2LaCl_5 . Transi-

tions from the lowest crystal-field level of ${}^4I_{9/2}$ to the five crystal-field levels of ${}^4F_{9/2}$ can be observed and identified in the same spectral range around $14\,600\text{ cm}^{-1}$. The total splitting is reduced from 400 to 187 cm^{-1} for U^{3+} and Nd^{3+} , respectively. A reduction of about 50% is typical also for the crystal-field splitting of the other terms. From the relative energy differences and intensities it is possible to establish a one to one relationship between the five states $G1$ to $G5$ for U^{3+} and Nd^{3+} as shown in Fig. 4 and listed in Table II. This is a nice illustration that a description of f - f excited states in terms of ${}^{2S+1}L_J$ functions is meaningful for both Nd^{3+} and U^{3+} . In absolute terms the ${}^4F_{9/2}$ absorptions are about two orders of magnitude less intense for Nd^{3+} than for U^{3+} . As a consequence the radiative rates for f - f luminescence transitions are typically two orders of magnitude bigger for U^{3+} than Nd^{3+} . Radiative processes are more competitive against nonradiative relaxation processes in the U^{3+} system, see also Sec. IV D.

C. Variation along the series $\text{K}_2\text{LaX}_5:\text{U}^{3+}$ ($X=\text{Cl,Br,I}$)

In the region of $5f \rightarrow 6d$ transitions the principal trend along $\text{Cl} \rightarrow \text{Br} \rightarrow \text{I}$ observed in Fig. 1 is a redshift of the order 1000 cm^{-1} . This is attributed to an increase in the covalency of the U-X bond resulting in smaller electron repulsion and spin-orbit parameters in both the $5f$ and $6d$ shell.

In the elpasolite host lattice $\text{Cs}_2\text{NaYCl}_6$ a qualitative assignment of the absorptions in the $5f \rightarrow 6d$ region has been done.^{10,11} Despite the fact that in our host lattices the coordination is not octahedral we can expect a similar strength of the electron repulsion between $5f$ and $6d$ electrons as in $\text{Cs}_2\text{NaYCl}_6$. An assignment of individual bands in the f - d region is not possible in our systems, however, because of the very low site symmetry which precludes the calculation of the crystal-field splittings resulting from the $(6d)^1$ sub-configuration.

We start, as we did before, our discussion of the excited states arising from the $(5f)^3$ electron configuration by neglecting the crystal-field splitting. The observed slight redshift of the 4J_J , 4F_J , 4G_J , 4S_J , and 2H_J baricenter energies along the series $\text{Cl} \rightarrow \text{Br} \rightarrow \text{I}$ is ascribed to a slight reduction of the electron-repulsion parameters. Superimposed on this there is a similarly small reduction of the spin-orbit splitting within each ${}^{2S+1}L$ multiplet. Both are the result of an increase in covalency, Jørgensens nephelauxetic effect.²⁴ The effect is bigger between Br and I than between Cl and Br .

The crystal-field splitting within a ${}^{2S+1}L_J$ term also shows a decreasing trend along $\text{Cl} \rightarrow \text{Br} \rightarrow \text{I}$, see Table II and Fig. 3. The most simple explanation for this trend is the increase of the U-X distances and the resulting decrease of the purely electrostatic crystal field. The mean U-X distances are 283.6 , 298.8 , and 325.9 pm in K_2UX_5 ($X=\text{Cl,Br,I}$), respectively.¹⁷⁻¹⁹ A quantitative analysis of the observed splittings in terms of a theoretical crystal-field model is made difficult if not impossible by the low symmetry at the U^{3+} site. The site symmetry is C_s . The coordination is sevenfold with U-X distances ranging from 277.5 to 288.1 pm , 294.8 to 303.2 pm , and 319.9 to 334.2 pm in the Cl , Br , and I lattices, respectively.¹⁷⁻¹⁹

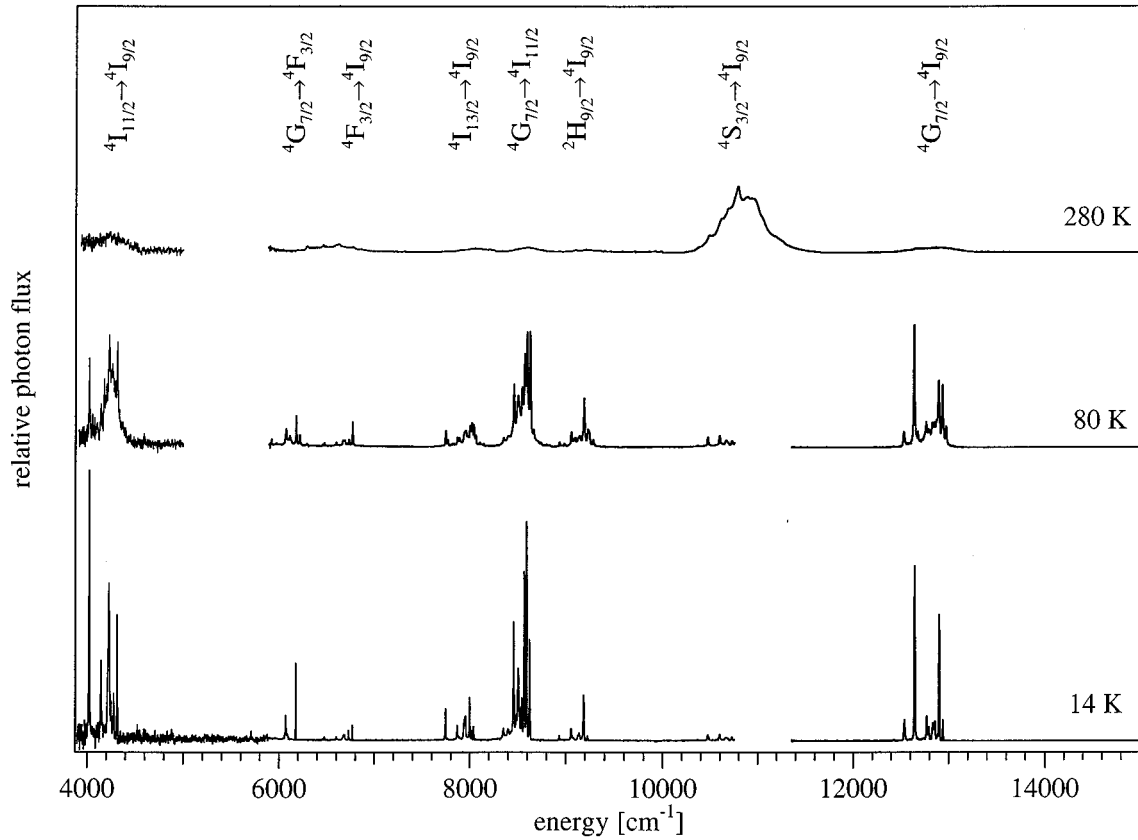


FIG. 5. Luminescence spectra of $\text{K}_2\text{LaI}_5:\text{U}^{3+}$ at $T = 14, 80,$ and 280 K. The gaps in the 14 and 80 K spectra are due to detector changes. Assignments of the multiplets are given at the top.

In Fig. 3, which shows the ${}^4G_{7/2} \rightarrow {}^4I_{9/2}$ transition in luminescence, we observe two additional trends which are typical also of other $f-f$ transitions. Besides the five electronic origins Z1 to Z5 to the five crystal-field components of the ${}^4I_{9/2}$ ground state, some vibrational sidebands can be clearly identified in the Br and I spectra. Their intensity increases along the series $\text{Cl} \rightarrow \text{Br} \rightarrow \text{I}$ as a result of an increase in the electron-phonon coupling. Each vibrational sideband is associated with an electronic origin, and we obtain vibrational energies of 250, 146, and 106 cm^{-1} for Cl, Br, and I, respectively. These are very close to the highest-energy vibrations identified by Raman spectroscopy in the host lattices: 235, 145, and 105 cm^{-1} , respectively.²⁵ They are assigned to U-X stretch vibrations. It is interesting to compare those vibrational energies with the highest-energy vibrations in fluoride ($\sim 350 \text{ cm}^{-1}$) and oxide ($\sim 550 \text{ cm}^{-1}$) lattices. Going down the halide series leads to an enormous reduction. Multiphonon relaxation processes will be directly affected by this. For a given energy gap they are least competitive in an iodide. Consequences of this will be discussed below in Sec. IV D.

TABLE IV. Luminescence lifetimes of ${}^4F_{3/2} \rightarrow {}^4I_{9/2}$ in μs for the three lattices.

	14 K	280 K
$\text{K}_2\text{LaCl}_5:\text{U}^{3+}$	600	530
$\text{K}_2\text{LaBr}_5:\text{U}^{3+}$	482	473
$\text{K}_2\text{LaI}_5:\text{U}^{3+}$	355	300

${}^4F_{3/2}$ is the only $f-f$ excited state which was found to decay single exponentially in all three lattices. Because of the large energy gap to the next lower ${}^4I_{11/2}$ multiplet we can take the experimental values in Table IV as radiative lifetimes. The observed decreasing trend both at 14 and 280 K along Cl, Br, I is in good accordance with an increase of the $f-d$ character in the $f-f$ excited states and the corresponding increase of the radiative $f-f$ transition rate constants.

D. Excited-state dynamics

The relaxation pathways after an initial excitation into the $f-d$ absorptions are determined by a complex interplay of radiative and nonradiative processes. We have two experimental handles to study these processes: the intensity distribution among the various luminescence transitions (Fig. 2 and Table III) and time-dependent measurements (Fig. 6 and Tables IV and V). In the following discussion two nonradiative processes will be considered: multiphonon relaxation on a single U^{3+} center and cross relaxation involving two

TABLE V. Measured luminescence lifetimes in μs of $\text{K}_2\text{LaI}_5:\text{U}^{3+}$ as a function of temperature.

T (K)	${}^4G_{7/2}$	${}^4S_{3/2}$	${}^2H_{9/2}$	${}^4I_{13/2}$	${}^4F_{3/2}$
14	10.8	19	46.3	77	355
80	10.7	16.6	41.9	67	328
280	1.2	14.6	38.2	65	300

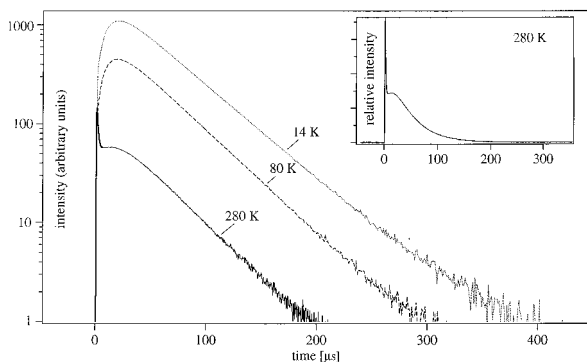


FIG. 6. Semilogarithmic rise and decay curves of the ${}^2H_{9/2} \rightarrow {}^4I_{9/2}$ luminescence in $K_2LaF_5:U^{3+}$ at three temperatures. The inset shows the ${}^2H_{9/2}$ transient in detail on a nonlogarithmic scale.

U^{3+} ions. In the multiphonon relaxation we have to further distinguish between the initial relaxation step from the $f-d$ excited state into the $f-f$ system and the subsequent steps down the ladder of $f-f$ states.

We start with the former and refer to Fig. 2. The highest-energy luminescence at 14 K in the Cl and Br lattices is ${}^4F_{9/2} \rightarrow {}^4I_{9/2}$, whereas for I it is ${}^4G_{7/2} \rightarrow {}^4I_{9/2}$. This difference is readily explained by the slightly lower position of the first $f-d$ state in the iodide. This is schematically illustrated in a single configurational coordinate picture in Fig. 7 where the coordinate represents an effective U-X stretch vibration. The $f-f$ and $f-d$ potentials are displaced along this coordinate, the $f-d$ state is more antibonding and thus has longer U-X equilibrium distances and a smaller force constant. As a consequence of this displacement the ${}^4F_{9/2}$ is by-passed nonradiatively in the iodide, see the right-hand side of Fig. 7. In the Cl and Br lattices, on the other hand, the $f-d$ potential is sufficiently elevated to prevent such a by-pass, see the left-hand side of Fig. 7.

For the interplay of radiative and nonradiative relaxation within the $f-f$ states, the discussion in Sec. IV C has revealed

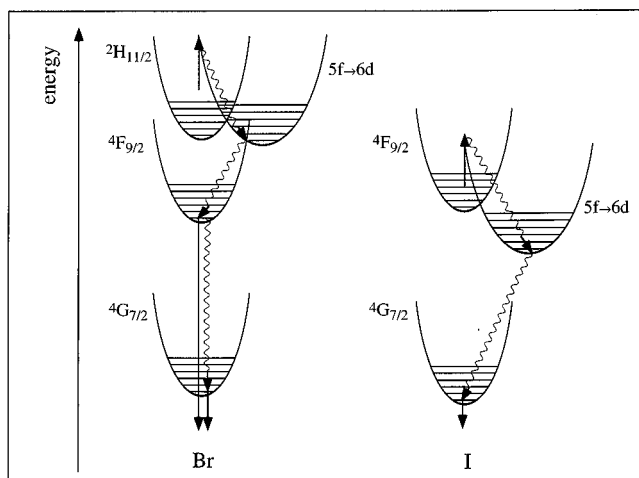


FIG. 7. Schematic configurational coordinate diagram for the lattices $K_2LaX_5:U^{3+}$ ($X=Br, I$) at the intersection of the $f-f$ states with the lowest $f-d$ state. Radiative and nonradiative processes are shown with full and sinusoidal arrows, respectively.

two important trends. There is an overall increase of about 30% in the radiative $f-f$ transition rate from Cl to I. The nonradiative multiphonon relaxation, on the other hand, strongly depends on the energy of accepting vibrations. The highest-energy vibrations decrease from 250 cm^{-1} in the Cl to 106 cm^{-1} in the I lattice. In lanthanide-doped systems the energy gap law²⁶ describes the situation adequately:

$$k_{mp} = C e^{-(\Delta E/\hbar\omega)\beta}$$

where k_{mp} is the multiphonon relaxation rate constant, ΔE is the energy gap from a given electronic state to the next-lower state, $\hbar\omega$ is an effective energy of the accepting mode, and β and C are positive-definite constants characteristic of the material. As a rule of thumb in lanthanide spectroscopy it is found that multiphonon relaxation processes are competitive when $p = \Delta E/\hbar\omega$, the number of phonons needed to bridge the electronic energy gap is smaller than six.²⁶ From Table II we see that several energy gaps between excited multiplets are of the order of a few hundred to 2000 wave numbers. On the basis of the energy gap law we therefore expect differences between the Cl, Br, and I lattices. This is indeed the case, as seen in Fig. 2 and Table III. Transitions from the ${}^4G_{7/2}$ excited state make a dominant contribution to the luminescence at 14 K only in the iodide, whereas multiphonon relaxation processes down to ${}^2H_{9/2}$ (bromide) and further to ${}^4F_{3/2}$ (chloride) are dominant in the other lattices. The energy gap between the ${}^4G_{7/2}$ and ${}^4F_{7/2}$ multiplets is between 1200 and 1300 cm^{-1} , small enough for efficient multiphonon relaxation in the chloride ($p \approx 4$) and bromide ($p \approx 8$), but not the iodide ($p \approx 13$). For the ${}^2H_{9/2}$ excited state we have a gap of $800\text{--}900\text{ cm}^{-1}$ to the next lower state, corresponding to $p \approx 3$ and ≈ 6 for the Cl and Br, respectively. In this case radiative processes compete successfully in the bromide, but not in the chloride.

The luminescence lifetimes observed in the I lattice, which are listed in Table IV, are therefore purely radiative lifetimes. They typically decrease by about 20% between 14 and 280 K as a result of a corresponding increase of the total radiative rate when higher crystal-field levels are populated. There is one notable exception, the ${}^4G_{7/2}$ lifetime drops by an order of magnitude between 80 and 280 K. Figure 5 and Table III show that this is accompanied by a corresponding drop of the ${}^4G_{7/2}$ luminescence intensity and an enormous increase of the ${}^4S_{3/2}$ luminescence. The latter dominates the 280 K luminescence spectra of the iodide. A fourth coinciding observation is shown in Fig. 6. At 280 K the decay curve of the ${}^2H_{9/2}$ luminescence has a strong and very fast component of about $1\text{ }\mu\text{s}$ or faster (see inset) before settling into the “normal” decay time of about $40\text{ }\mu\text{s}$.

All these observations can be explained with the cross-relaxation process shown in Fig. 8. Two excited U^{3+} ions, one in ${}^4G_{7/2}$ and one in ${}^2H_{9/2}$, close enough in the crystal lattice to exchange part of their excitation energy, can cross relax into two states within the box [${}^4S_{3/2}$, ${}^4G_{5/2}$, ${}^4I_{15/2}$, ${}^4F_{7/2}$]. Such a process requires at least two steps in such a diluted crystal. In step 1 the ${}^4G_{7/2}$ and ${}^2H_{9/2}$ excitations migrate resonantly through the lattice until the cross-relaxation step can take place. Both steps are expected to be more efficient at higher temperatures, in agreement with the observed behavior. The energy migration by an electric dipole-

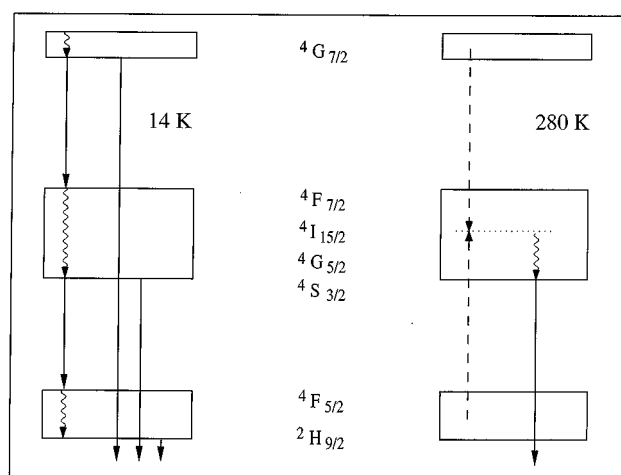


FIG. 8. A schematic presentation of the relaxation processes in $K_2LaI_5:U^{3+}$ at 14 K (left) and 280 K (right) after $^4G_{7/2}$ excitation. The full and sinusoidal arrows are indicating radiative and nonradiative processes, respectively. The dashed arrows show one possible cross-relaxation process at 280 K.

dipole mechanism becomes more probable because the oscillator strengths of the higher crystal-field components of the $^4G_{7/2}$ and $^2H_{9/2}$ excitations are higher as shown by a detailed examination of the absorption spectra. The cross-relaxation step itself becomes more probable because according to Table II there are six energy matches within 2 cm^{-1} at 280 K, in contrast to only one at 14 K. These can be considered as resonant and thus particularly efficient. After the cross-relaxation process fast multiphonon relaxation down to $^4S_{3/2}$ will occur, leading to $^4S_{3/2}$ luminescence as observed. It is remarkable that in such a diluted crystal (the actual U^{3+} concentration is expected to be smaller than 1%) a cooperative effect can become so dominant with a rate constant of at least 10^6 s^{-1} . It is most likely an electric dipole-dipole transfer process, which is long-range and dependent on the oscillator strengths of the relevant electronic transitions. Since these are about two orders of magnitude greater than in lanthanides, such a transfer process is about four orders of magnitude more efficient for a given distance between donor

and acceptor. The relatively large number of possible (near) resonant transfer processes is due to the fact that all crystal-field levels of $^4G_{7/2}$ and $^2H_{9/2}$ are populated at 280 K. At 14 K only the levels $F1(^4G_{7/2})$ and $A1(^2H_{9/2})$ are appreciably populated thus reducing drastically the number of (near) resonant energy transfer pathways. This is in excellent agreement with the experiment, see Fig. 5. We cannot exclude the possibility that the U^{3+} ions are not statistically distributed. The very efficient cross-relaxation might be the result of a clustering of the U^{3+} ions.

The population of $^4I_{11/2}$ occurs radiatively at 14 K in all three lattices. The emitting states are $^4F_{3/2}$, $^4I_{13/2}$, and $^4G_{7/2}$ in Cl, Br, I, respectively. The former two transitions are in the infrared beyond 4000 cm^{-1} , they were not observed. The $^4G_{7/2} \rightarrow ^4I_{11/2}$ luminescence is dominant in the I spectrum at 14 K, see Fig. 2.

V. CONCLUSIONS

In conclusion, we have found that the variation of the chemical environment of U^{3+} without changing the structure provides considerable insight into the electronic structure, the nature of the excited states, and the interplay of radiative and nonradiative relaxation mechanisms. It is by the observation of the trends along the series $K_2LaX_5:U^{3+}$ ($X=Cl, Br, I$) that we can rationalize and understand the relevant excited-state properties.

We have deliberately not attempted to fit the observed energies with a theoretical model based on an effective Hamiltonian as was done in Refs. 4, 6–9, and 16. For an ion such as U^{3+} these are essentially descriptive models with parameters which are very difficult if not impossible to interpret physically. We therefore prefer to interpret the trends in the observables.

ACKNOWLEDGMENTS

We thank T. C. Brunold, A. Hauser, M. F. Hazenkamp, and T. Riedener for their support in the spectroscopy. This project was financially supported by the Swiss National Science Foundation.

¹W. A. Hargreaves, G. D. Boyd, R. J. Collins, S. P. S. Porto, and A. Yariv, *Phys. Rev. Lett.* **8**, 269 (1962).

²W. A. Hargreaves, *Phys. Rev.* **156**, 331 (1967).

³W. A. Hargreaves, *Phys. Rev. B* **44**, 5293 (1991).

⁴J. Drożdżyński and J. G. Conway, *J. Chem. Phys.* **56**, 883 (1972).

⁵J. P. Hessler, J. Hegarty, C. G. Levey, G. F. Imbush, and W. M. Yen, *J. Lumin.* **18-19**, 73 (1979).

⁶J. B. Gruber, J. R. Morney, and P. G. Carter, *J. Chem. Phys.* **71**, 3982 (1979).

⁷H. M. Crosswhite, H. Crosswhite, W. T. Carnall, and A. P. Paszek, *J. Chem. Phys.* **72**, 5103 (1980).

⁸W. T. Carnall, *J. Chem. Phys.* **96**, 8713 (1992).

⁹T. Tröster, W. B. Holzappel, and J. Goffert, *Phys. Rev. B* **51**, 14 892 (1995).

¹⁰Z. Mazurak, J. Drożdżyński, and J. Hanuza, *J. Mol. Struct.* **174**, 443 (1988).

¹¹J. Drożdżyński, *Acta. Phys. Pol. A* **84**, 975 (1993).

¹²P. J. Dereń, W. Strek, and J. Drożdżyński, *J. Mol. Struct.* **325**, 149 (1994).

¹³G. Quarles, L. Esterowitz, G. H. Rosenblatt, R. Uhrin, and R. F. Belt, *OSA Proceedings on Advanced Solid-State Lasers* (Optical Society of America, Washington, DC, 1993), Vol. 13, p. 306.

¹⁴H. P. Jensen, M. A. Naginov, and A. Cassanho, *OSA Proceedings on Advanced Solid-State Lasers* (Optical Society of America, Washington, DC, 1993), Vol. 15, p. 463.

¹⁵S. Hubert, E. Simoni, M. Louis, W. P. Zhang, and J. Y. Gesland, *J. Lumin.* **60-61**, 245 (1994).

¹⁶E. Simoni, M. Louis, J. Y. Gesland, and S. Hubert, *J. Lumin.* **65**, 153 (1995).

¹⁷K. Krämer, L. Keller, P. Fischer, B. Jung, N. N. Edelstein, H. U. Güdel, and G. Meyer, *J. Solid State Chem.* **103**, 152 (1993).

¹⁸K. Krämer, H. U. Güdel, G. Meyer, T. Heuer, N. N. Edelstein, B.

- H. Jung, L. Keller, P. Fischer, E. Zych, and J. Drożdżyński, *Z. Anorg. Allg. Chem.* **620**, 1339 (1994).
- ¹⁹L. Keller, A. Furrer, P. Fischer, P. Allenspach, K. Krämer, H. U. Güdel, A. Dönni, and T. Suzuki, *Phys. Rev. B* **51**, 2881 (1995).
- ²⁰G. Meyer, *Inorg. Synth.* **25**, 146 (1989).
- ²¹G. Meyer, *Synthesis of Lanthanide and Actinide Compounds*, edited by G. Meyer and L. Morss (Kluwer, Dordrecht, 1991), p. 145.
- ²²E. Ejder, *J. Opt. Soc. Am.* **59**, 223 (1969).
- ²³H. M. Crosswhite, H. Crosswhite, F. W. Kasetta, and R. Sarup, *J. Chem. Phys.* **64**, 1981 (1976).
- ²⁴R. Reisfeld and C. K. Jørgensen, *Lasers and Excited States of Rare Earths* (Springer-Verlag, Berlin, 1977), p. 124.
- ²⁵K. Krämer, and H. U. Güdel, *J. Alloys Compounds* **207-208**, 128 (1994).
- ²⁶L. A. Riseberg and H. W. Moos, *Phys. Rev.* **174**, 429 (1968).